Computers in Biology and Medicine 138 (2021) 104912

Contents lists available at ScienceDirect

Computers in Biology and Medicine

journal homepage: www.elsevier.com/locate/compbiomed

Modeling indoxyl sulfate transport in a bioartificial kidney: Two-step binding kinetics or lumped parameters model for uremic toxin clearance?

Jasia King [a], Sangita Swapnasrita [a], Roman Truckenmüller [a], Stefan Giselbrecht [a], Rosalinde Masereeuw [b], Aurélie Carlier [a,*]

[a] MERLN Institute for Technology-Inspired Regenerative Medicine, Maastricht University, 6229 ER Maastricht, the Netherlands
[b] Division of Pharmacology, Utrecht Institute for Pharmaceutical Sciences, Utrecht University, 3584 CG Utrecht, the Netherlands

ARTICLE INFO

Keywords:
Modeling
Membranes
Kinetics
Hollow fiber membrane
Indoxyl sulfate
Organic anion transporters

ABSTRACT

Toxin removal by the kidney is deficient in a patient suffering from end-stage kidney disease (ESKD), and current dialysis therapies are insufficient in subsidizing this loss. A bioartificial kidney (BAK) aspires to offer ESKD patients a more effective alternative to dialysis. Mathematical models are necessary to support further developments and improve designs for the BAK before clinical trials. The BAK differentiates itself from dialysis by incorporating a living proximal tubule cell monolayer to account for the active transport of protein-bound uremic toxins, namely indoxyl sulfate (IS) in this study. Optimizing such a device is far from trivial due to the non-intuitive spatiotemporal dynamics of the IS removal process. This study used mathematical models to compare two types of active transport kinetics. i.e., two-step binding and lumped parameter. The modeling results indicated that the transporter density is the most influential parameter for the IS clearance. Moreover, a uniform distribution of transporters increases the IS clearance, highlighting the need for a high-quality, functional proximal tubule monolayer in the BAK. In summary, this study contributed to an improved understanding of IS transport in the BAK, which can be used along with laboratory experiments to develop promising renal replacement therapies in the future.

1. Introduction

It was estimated in 2017 that approximately 697.5 million people suffered from chronic kidney disease, with only 2.5 million receiving treatment worldwide [1,2]. Kidney transplantation is the treatment of preference for final stages of CKD, followed by dialysis as a bridge to transplantation. Unfortunately, both treatment options have their limitations. Kidney transplantation has limited availability, some patients cannot be transplanted due to complications, and a donor organ may not be affordable to everyone [2]. On the other hand, dialysis mimics the kidney's filtration function and only partially removes endogenous waste (also named uremic toxins) such as small, water-soluble and middle molecules from the patient's circulation [3,4]. The proximal tubule (PT) function cannot be recapitulated in dialysis, which results in an accumulation of large, protein-bound uremic toxins (PBUT) that require active transport for their removal [5,6]. One of these accumulated PBUTs is indoxyl sulfate (IS), associated with lower drug binding, anemia, insulin resistance, epileptic seizures, and kidney failure progression, among many other comorbidities [6,7]. The molecular weight of this PBUT is typically less than 500 Da when unbound. However, more than 90% of the IS molecules form strong bonds with albumin in the blood circulation, resulting in a complex greater than 65 kDa which is too large for filtration and dialysis [4,5]. IS interacts with a plethora of transporters classified as solute carriers (SLCs) and ATP-binding cassette families that are responsible for their trans-epithelial transport. PBUTs are typically taken up by the PT cells via SLC transporters at their basolateral membrane, in particular the Organic Anionic Transporter (OAT) 1 and, to a lesser extent, OAT3 [8,9]. Next, ABC transporters are responsible for their transfer from PT cells into the urinary compartment [9]. The absence of active toxin transport in traditional dialysis is one of the main reasons for their reduced clearance.

Although improvements have been made to advance membranes since the technology's invention in the 1950s, dialysis remains a passive mass transport process. A bioartificial kidney (BAK) could present an effective alternative to dialysis by incorporating a living proximal tubule

* Corresponding author.
E-mail address: a.carlier@maastrichtuniversity.nl (A. Carlier).

https://doi.org/10.1016/j.compbiomed.2021.104912
Received 16 July 2021; Received in revised form 20 September 2021; Accepted 28 September 2021
Available online 1 October 2021

cell monolayer to account for the active transport of protein-bound uremic toxins. For example, Jansen et al. cultured conditionally immortalized proximal tubule epithelial cells with the overexpression of OAT1 (ciPTEC-OAT1) *in vitro* on dialysis hollow fiber membranes and demonstrated active transepithelial IS transport [10].

To replicate and supplement the *in vitro* transport phenomena studies of Jansen et al., in 2016 [10], Refoyo et al. developed a computational model of IS crossing a ciPTEC-OAT1 monolayer cultured on a single hollow fiber [11]. More specifically, Refoyo et al. created a four-compartment model including a blood compartment, the hollow fiber membrane, the ciPTEC-OAT1 monolayer and a dialysate compartment to simulate the spatiotemporal dependencies of IS as it is transported from the blood to the dialysate. The IS binds to albumin in the bloodstream to form a complex, which can cross the porous membrane of the hollow fibers to approach the cell monolayer. Here, OAT1 can take over the IS which dissociates from the plasma protein to be transported into the cytoplasm. Eventually, IS expelled into the dialysate. The interaction between OAT1 and IS is modeled with lumped parameter Michaelis-Menten (MM) kinetics at the cell membrane. Although MM kinetics may be a good approximation for toxin-transporter binding, the resulting (lumped) model loses the specificity of the binding and dissociation step when it is assumed as a general inward flux for the toxin transport. Moreover, the lumped model also does not allow simulating the influence of an inhibitor or activator of the competitive binding kinetics with another toxin. Since renal transporters are essential for body homeostasis, understanding the mechanisms of action of individual transporters is essential to make an effective patient-specific treatments.

In this study, we proposed and investigated an alternative distributed parameterized computational model that assumes that OAT1 interacts with IS as a model toxin in a two-step process involving the separation of the flux boundary condition into an OAT1 density and activity along the cell membrane. We also compared the use of lumped surface parameters [11] and two-step binding kinetics for adequate toxin clearance from the bloodstream, hereafter referred to as 'Lumped Model' and 'Two-Step Binding Kinetics Model' (TSKM), respectively. As such, this study contributes to an improved understanding of IS transport through the wall of cell-laden hollow fibers, which can help in developing a strategy for the removal of uremic toxins in renal replacement therapies.

2. Materials and methods

Both the Lumped Model and the TSKM were developed as described in Refoyo et al. [11] using COMSOL Multiphysics 5.4. Simulations were performed with an "extra fine" mesh in both cases with a total computational time of 1.75 min using the inbuilt time-dependent study solved using the Configurations Solver which stored the solution of multiple nodes and allowed the simulations to use a sequence of subnodes to compute the simulation. The models were *in silico* representations of the continuously perfused hollow fiber cultured with a monolayer of ciPTEC-OAT1 as established by Jansen et al., in 2016 [10], described in more detail in the following sections. Both models consisted of the above-introduced four compartments – blood, porous membrane, cell monolayer, and dialysate. The flux of toxins is described in all four compartments. We compared the two types of kinetics involved in the transfer of the toxin from the membrane into the dialysate via the cell monolayer in the presence of albumin in the bloodstream.

2.1. Geometry

The schematic of a dialysis filter unit shown in Fig. 1A was comprised of the hollow fiber bundles (Fig. 1B) that are used to culture the ciPTEC-OAT1 monolayer, then used to make the BAK. The *in silico* model was divided into four compartments: blood, hollow-fiber membrane, ciPTEC-OAT1 cell monolayer, and dialysate. Each compartment was added as an axisymmetric rectangular subdomain with the dimensions shown in Fig. 1C. The interactions of the IS, serum albumin and OAT1 at the basolateral cell membrane were summarized in Fig. 1D.

2.2. Physics description

The general reaction-diffusion-convection transport equation was applied to all compartments of the models, similar to Refoyo et al. [11], where Table 1 lists the subscripts used in the model definition.

2.2.1. Blood compartment

Equations 1a, 1b and **2** were the implementation of the transport of IS in the blood compartment, including diffusion, convection, and binding kinetics of albumin and IS.

$$\frac{\partial C_{is,b_{bound}}}{\partial t} - \underbrace{D_{is,b_{bound}}\nabla^2 C_{is,b_{bound}}}_{\text{Diffusion}} + \underbrace{u_{z_b}\nabla C_{is,b_{bound}}}_{\text{Convection}} = \underbrace{\mathscr{R}_{is,b_{bound}}}_{\text{Reaction}} \tag{1a}$$

$$\frac{\partial C_{is,b_{free}}}{\partial t} - \underbrace{D_{is,b_{free}}\nabla^2 C_{is,b_{free}}}_{\text{Diffusion}} + \underbrace{u_{z_b}\nabla C_{is,b_{free}}}_{\text{Convection}} = \underbrace{\mathscr{R}_{is,b_{free}}}_{\text{Reaction}} \tag{1b}$$

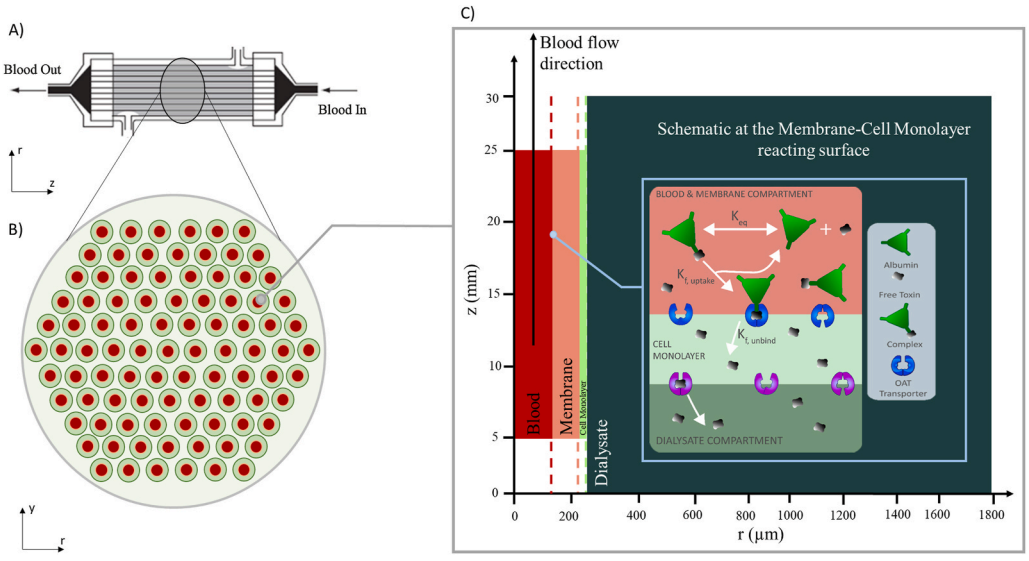

Fig. 1. (A) Minimal schematic of BAK unit. (B) Cross-section of the BAK to show the hollow fiber orientation and cell-laden device (C) Geometry implementation of the hollow fiber, showing here an axisymmetric implementation of one fiber. The schematic figure displays the dimensions for each compartment and the flux direction of the toxins. Flow was restricted to the blood compartment. The interactions among IS, serum albumin, and the OAT1 at the basolateral cell membrane (membrane-cell monolayer boundary) is described in the blue box. The colors of the compartments match with the colors in geometry definitions of 1B: Blood compartment in red, membrane compartment in pink, cell monolayer in light green and dialysate in dark green.

Table 1
Subscripts used in the model definition.

Subscripts	Meaning
A	Albumin
b	Blood domain
m	Membrane domain
c	Cell monolayer domain
d	Dialysate domain
r	In the radial direction
z	In the axial direction
uptake	Binding of toxin to transporter
unbind	Dissociation of toxin from transporter
bound	Bound toxin/transporter
free	Free toxin/transporter
s	Surface

$$u_{z_b} = u_{\max}\left(1 - \left(\frac{r}{R_b}\right)^2\right) \tag{2}$$

where $C_{is_{b,bound}}$ and $C_{is_{b,free}}$ was the concentration of bound and free IS in the blood compartment, $D_{is_{b,bound}}$ and $D_{is_{b,free}}$ was the diffusion coefficient of bound and free IS in the blood, u_{z_b} was the velocity applied to the blood compartment (see Equation (2)), and $\mathscr{R}_{is_{b,free}}$ was the reaction of the association and dissociation of albumin with IS in the blood compartment assuming $K_{eq} = 377$ mol m^{-3} for the equilibrium constant. The equilibrium reaction equation is

$$c_{is,b_{free}} + c_A \leftrightarrow^{k_{eq}} c_{is,b_{bound}} \tag{3}$$

where $c_{is,b_{free}}, c_A, c_{is,b_{bound}}$ are the concentration of indoxyl sulfate (IS), free albumin and albumin-IS complex in the blood stream. The equilibrium reaction was used to initialize the model's ratio of bound and unbound concentration of IS, resulting in $\mathscr{R}_{is_{b,bound}} = 0$and $\mathscr{R}_{is_{b,free}} = 0$ for the duration of the simulation. The flow in the compartment was a laminar flow with the maximum velocity found at the center and zero velocity at the edges.

2.2.2. Membrane compartment

Similarly, **Equation 4a and b** was implemented to describe the diffusion and binding kinetics of albumin and IS in the porous hollow fiber membrane compartment.

$$\frac{\partial C_{is,m_{bound}}}{\partial t} - D_{is,m_{bound}}\nabla^2 C_{is,m_{bound}} = \mathscr{R}_{is,m_{bound}} \tag{4a}$$

$$\frac{\partial C_{is,m_{free}}}{\partial t} - D_{is,m_{free}}\nabla^2 C_{is,m_{free}} = \mathscr{R}_{is,m_{free}} \tag{4b}$$

where $C_{is,m_{bound}}$ and $C_{is,m_{free}}$ was the concentration of bound and free IS in the membrane compartment, $D_{is,m_{bound}}$ and $D_{is,m_{free}}$ was the diffusion coefficient of IS in the membrane, and $\mathscr{R}_{is,m_{bound}}$ and $\mathscr{R}_{is,m_{free}}$ was the reaction of the association and dissociation of albumin with IS in the membrane compartment assuming the same equilibrium constant as for the blood compartment ($K_{eq} = 377$ mol m^{-3} as shown in equation (3)). The equilibrium reaction was used to initialize the model's ratio of bound and unbound concentration of IS, resulting in $\mathscr{R}_{is_{b,bound}} = 0$and $\mathscr{R}_{is_{b,free}} = 0$, for the duration of the simulation.

2.2.3. Cell monolayer and dialysate compartment

Unbound and bound IS are transported across the basolateral cell membrane into the cell monolayer. The cells were assumed to be uniformly distributed in the cell monolayer compartment. The toxin transport within the cell monolayer and dialysate was considered diffusion-dependent (**Equations 5 & 6**). Since albumin was not transported across the membrane, we have removed the reaction term.

$$\frac{\partial C_{is,c_{free}}}{\partial t} - D_{is,c_{free}}\nabla^2 C_{is,c_{free}} = 0 \tag{5}$$

$$\frac{\partial C_{is,d_{free}}}{\partial t} - D_{is,d_{free}}\nabla^2 C_{is,d_{free}} = 0 \tag{6}$$

2.3. Boundary conditions at the membrane-monolayer interface for the lumped model

In Refoyo et al. [11], flux continuity was assumed at the blood-membrane and cell monolayer-dialysate interfaces,

$$D_{is,b_{bound}}\left(\frac{\partial C_{is,b_{bound}}}{\partial r}\right)_{r=R_b} = -D_{is,m_{bound}}\left(\frac{\partial C_{is,m_{bound}}}{\partial r}\right)_{r=R_m} \tag{7a}$$

$$D_{is,b_{free}}\left(\frac{\partial C_{is,b_{free}}}{\partial r}\right)_{r=R_b} = -D_{is,m_{free}}\left(\frac{\partial C_{is,m_{free}}}{\partial r}\right)_{r=R_m} \tag{7b}$$

$$D_{is,c_{free}}\left(\frac{\partial C_{is,c_{free}}}{\partial r}\right)_{r=R_c} = -D_{is,d_{free}}\left(\frac{\partial C_{is,d_{free}}}{\partial r}\right)_{r=R_d} \tag{8}$$

The flux boundary condition at the membrane-cell monolayer was modeled as a MM uptake kinetics of the OAT1 transporter (**Equation 9a and b**) with $K_m$and $V_{\max}$ as parameters. The Michaelis-Menten constant, $K_m$represents the affinity factor of IS for OAT1, or mathematically, the concentration of IS at which the reaction rate is half of the maximum, $V_{\max}$. Refoyo et al. calibrated K_m and $V_{\max}$ to obtain similar clearances as in the reported *in vitro* experiments.

$$D_{is,m_{bound}}\left(\frac{\partial C_{is,m_{bound}}}{\partial r}\right)_{r=R_m} = \frac{V_{\max}\, C_{is,m_{bound}} f}{K_m + C_{is,m_{bound}}} = D_{is,c_{free}}\left(\frac{\partial C_{is,c_{free}}}{\partial r}\right)_{r=R_c} \tag{9a}$$

$$D_{is,m_{free}}\left(\frac{\partial C_{is,m_{free}}}{\partial r}\right)_{r=R_m} = \frac{V_{\max}\, C_{is,m_{free}}}{K_m + C_{is,m_{free}}} f = D_{is,c_{free}}\left(\frac{\partial C_{is,c_{free}}}{\partial r}\right)_{r=R_c} \tag{9b}$$

To incorporate the MM flux condition, which represents a surface reaction, a form factor, f was used. The form factor was the local volume to area ratio at the reacting boundary (membrane and basolateral cell membrane). In this model, f was taken as 0.85 μm.

However, in the TSKM, the flux boundary condition was assumed to be a series of binding and dissociation surface reactions.

2.4. Defining the flux boundary condition for the membrane-cell monolayer interface in two-step binding kinetics model

We have assumed flux continuity at the blood-membrane interface. A two-step dissociation and binding reaction was assumed at the porous membrane-to-basolateral cell membrane boundary. In the TSKM, OAT1 was explicitly modeled along the boundary as a surface concentration with negligible diffusion along the membrane by pairing the surface reaction and chemistry modules in COMSOL Multiphysics 5.4. More specifically, OAT1 was considered in two states: unbound and bound to IS. OAT1 took up the bound and unbound form of IS via chemical reaction 1 and 2 (as seen in Table 2) and released the IS into the cell monolayer compartment via chemical reaction 3 and 4 (Fig. 1C and D

Table 2
Reactions of the two-step binding kinetics model on the basolateral side of the cell monolayer reacting with OAT. All subscripts are defined in Table 1.

Reaction Equation	Reaction Rate	Interface
$is_{bound} + OAT_{free} \rightarrow OAT_{bound} +$ Albumin	$k_{f_{uptake}} \times C_{is,m_{bound}} \times OAT_{free}$	Membrane-cell monolayer
$is_{free} + OAT_{free} \rightarrow OAT_{bound}$	$k_{f_{uptake}} \times C_{is,m_{free}} \times OAT_{free}$	Membrane-cell monolayer
$OAT_{bound} \rightarrow OAT_{free} + is_{free}$	$k_{f_{unbind}} \times OAT_{bound}$	Membrane-cell monolayer

and Table 2). Both reactions used mass action kinetics, a forward rate constant $k_{f_{uptake}}$ and similarly for backward rate, $k_{f_{unbind}}$. Mass flux was defined at membrane-monolayer boundary on the blood side as stated in Equations 10a, 10b, 11a, 11b and 12. Supporting Fig. 2 illustrated the location and detailed equations at the membrane-cell monolayer interface for both the TSKM and Lumped Model. The TSKM COMSOL model is available upon request.

At the membrane-cell monolayer interface, the inward flux was implemented as,

$$-D_{is,m_{bound}}\left(\frac{\partial C_{is,m_{bound}}}{\partial r}\right)_{r=R_m} = -\left(k_{f_{uptake}} \times C_{is,m_{bound}} \times OAT_{free}\right) \quad (10a)$$

$$-D_{is,m_{free}}\left(\frac{\partial C_{is,m_{free}}}{\partial r}\right)_{r=R_m} = -\left(k_{f_{uptake}} \times C_{is,m_{free}} \times OAT_{free}\right) \quad (10b)$$

$$\mathscr{R}_{Albumin} = \left(k_{f_{uptake}} \times C_{is,m_{bound}} \times OAT_{free}\right)$$

$C_{is,m_{bound}}$ is the albumin bound IS reacting with the free OAT on the membrane-cell monolayer reacting surface, $C_{is,m_{free}}$ is the albumin free IS reacting with the free OAT on the membrane-cell monolayer reacting surface, OAT_{free} is the OAT along the membrane-cell monolayer reacting surface that was free to bind with IS, OAT_{bound} is the OAT along the membrane-cell monolayer reacting surface that was bound with IS.

Flux was also conserved at the surface for OAT1, as the transporter remains only on the interface between the membrane and the cell monolayer (see supporting Fig. 2 for more a visual representation).

$$\frac{\partial C_{s,OAT_{bound}}}{\partial t} + \nabla\left(-D_{s,OAT_{bound}}\nabla C_{s,OAT_{bound}}\right) = \left(k_{f_{uptake}} \times OAT_{free} \times \left(C_{is,m_{bound}} + C_{is,m_{free}}\right)\right) - \left(k_{f_{unbind}} \times OAT_{bound}\right) \quad (11a)$$

$$\frac{\partial C_{s,OAT_{free}}}{\partial t} + \nabla\left(-D_{s,OAT_{free}}\nabla C_{s,OAT_{free}}\right) = -\left(k_{f_{uptake}} \times OAT_{free} \times \left(C_{is,m_{bound}} + C_{is,m_{free}}\right)\right) + \left(k_{f_{unbind}} \times OAT_{bound}\right) \quad (11b)$$

where.

$C_{s,OAT_{free}}$ and $C_{s,OAT_{bound}}$ are the IS free (or available) and IS bound (or unavailable) transporter density in mol m^{-2}, at the membrane-monolayer interface at the reacting surface.

At the membrane-monolayer interface on the monolayer side, the flux condition was

$$-D_{is,c_{free}}\left(\frac{\partial C_{is,c_{free}}}{\partial r}\right)_{r=R_c} = k_{f_{unbind}} \times OAT_{bound} \quad (12)$$

The monolayer-dialysate interface has a boundary condition specified as a flux continuity defined in equation (8).

2.5. Parameter fitting

In order to compare the two types of kinetics, the base parameter values for the TSKM, i.e. transporter uptake rate ($k_{f_{uptake}}$), transporter unbind rate ($k_{f_{unbind}}$) and initial transporter density (OAT_{free}), were chosen as the combination that predicts the same toxin clearance as that observed in the Refoyo kinetics. In particular, one parameter was varied while keeping the other parameter values constant. It started with an excess of dissociation rate (10 s^{-1}) and initial transporter density (1e-2 mol m^{-2}) under the assumption that the ciPTEC-OAT1 cell line overexpresses OAT1 and the protein would not be the limiting factor of IS transport. First alterations were made to increase transporter uptake rate (1e-3 m^3 s^{-1} mol^{-1}) while the other two parameters were held constant. The uptake rate was increased until there were no further changes in the resulting IS concentration profile. Similar step changes were done with transporter unbind rate, where the parameter was decreased while holding the uptake rate and transporter density constant. Finally, the transporter density was decreased from the oversaturated condition until the IS concentration profile closer resembled that of the Lumped Model. By carefully studying the parameters like this, we were able to arrive at a base configuration of parameters as shown in Table 3, which predict the same toxin clearance as that observed in the Lumped Model and are in a similar order of magnitude as mentioned in literature [12].

2.6. Sensitivity analysis

A sensitivity analysis was performed on the TSKM where the individual parameters were altered to investigate which parameter was most influential on the clearance of IS. The sensitivity analysis was performed on the TSKM for the transporter density, uptake and unbind rate for a ±

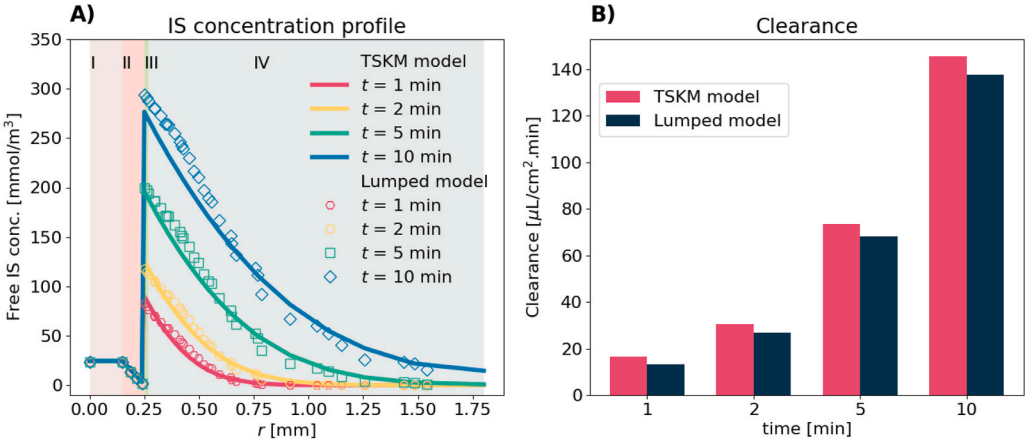

Fig. 2. Panel view comparing the TSKM's and Lumped Model's cross-section at $z = 10$ mm. We focus here on the first 10 min, comparable to Refoyo et al. (A) Toxin concentration profile at different time steps for the Lumped Model [11] and TSKM using the parameters in Table 3. All domains are highlighted in Fig. 1A. (I) Blood: $r <$ 0.15 mm; (II) Porous membrane: 0.15 $< r <$ 0.25 mm; (III) Cell monolayer: 0.25 $< r <$ 0.27 mm; (IV) Dialysate: $r >$ 0.27 mm. The y-axis units are converted to mmol m^{-3} to better represent the data in graphical format. (B) Clearance of albumin-bound and albumin-free IS as predicted by both models.

Table 3
Parameters used to develop the Lumped Model [11] and Two-Step Binding Kinetics model.

Model parameter			
Parameter name (variable used)	Value	Unit	Reference
Flowrate	1.667e-9	$m^3\ s^{-1}$	[10]
IS diffusion coefficient in the blood ($D_{is_{b,bound}}$ *or* $D_{is_{b,free}}$)	5.58309e-10	$m^2\ s^{-1}$	[13]
IS diffusion coefficient in the cell compartment ($D_{is,c}$)	5.58309e-10	$m^2\ s^{-1}$	[13]
IS diffusion coefficient in the dialysate (D_{is_d})	5.58309e-10	$m^2\ s^{-1}$	[13]
OAT diffusion coefficient in the membrane ($D_{s,OAT_{bound}}$ *or* $D_{s,OAT_{free}}$)	0	$m^2\ s^{-1}$	–
Membrane porosity (e)	0.45	unitless	[14]
IS diffusion coefficient in the porous membrane ($D_{is_{m,bound}}$ *or* $D_{is_{m,free}}$))	$D_{is_b} \times e$	$m^2\ s^{-1}$	[13]
Initial IS free concentration in blood and membrane ($C_{is,b_{free}}$ *or* $C_{is,m_{free}}$)	24.67	μM	[11]
Initial IS bound concentration in blood and membrane ($C_{is,b_{bound}}$ *or* $C_{is,m_{bound}}$)	73.33	μM	[11]
Initial IS_{free} concentration in cell monolayer and dialysate($C_{is,c_{free}}$ *or* $C_{is,d_{free}}$)	0	μM	–
Maximum inlet velocity in blood (u_{max})	0.047	m s^{-1}	[10]
Lumped Model (MM kinetics)			
Maximum rate (V_{max})	1.667e10	μmol $m^3\ s^{-1}$	[11]
Half of maximum concentration (K_m)	1e6	μmol m^3	[11]
Two-Step Binding Kinetics model			
Transporter uptake rate ($k_{f_{uptake}}$)	1	$m^3\ s^{-1}\ mol^{-1}$	fitted
Transporter unbind rate ($k_{f_{unbind}}$)	0.1	s^{-1}	fitted
Transporter density free from IS concentration at the membrane-cell monolayer interface (OAT_{free})	7e-5	mol m^{-2}	fitted
Transporter density bound to IS concentration at the membrane-cell monolayer interface (OAT_{bound})	0	mol m^{-2}	–
Geometry			
Height of the blood, membrane and cell monolayer domain (l)	0.02	m	[11]
Height of the dialysate domain	0.03	m	[11]
Radius of the blood compartment (R_b)	0.00015	m	[11]
Radius of the membrane compartment (R_m)	0.0001	m	[11]
Radius of the cell monolayer compartment (R_c)	0.00002	m	[11]
Radius of the dialysate compartment (R_d)	0.00153	m	[11]

20% change in each TSKM parameter stated in Table 3 using Equation (13).

$$\text{Sensitivity} = \frac{|CL(k) - CL(k+\Delta k)|}{CL(k)} \Big/ \frac{\Delta k}{k} \tag{13}$$

where.

$CL(k)$ = clearance value of the standard model.

$CL(k + \Delta k)$ = clearance with the varied parameter value.

Δk = variation in parameter value and

k = standard model parameter value.

In addition to the sensitivity analysis, to explore the effect of the parameter values on the IS clearance we multiplied the parameter values of interest by 0.01, 0.1 and 10 (Table 4), while holding the others at their original value in the TSKM.

Table 4
Parameters used to vary OAT1 uptake and dissociation kinetics and the density of OAT1 along the basolateral cell membrane. The parameters in bold represent the standard conditions.

Parameters [units]	Values
$k_{f_{uptake}}$ [$m^3\ s^{-1}\ mol^{-1}$]	0.01, 0.1, 1, 10
$k_{f_{unbind}}$ [s^{-1}]	0.001, 0.01, 0.1, 1
OAT_{free} [mol m^{-2}]	7e-7, 7e-6, 7e-5, 7e-4

3. Results

3.1. Similar clearance was shown in both models

By fitting the parameters to the TSKM, comparable toxin clearance with that of the *in silico* results of Refoyo et al. were achieved [11]. To directly compare the Refoyo et al. *in silico* results with the TSKM, the Lumped Model and TSKM, the free IS concentration in the blood, porous membrane, cell monolayer and the dialysate domain was simulated at different time steps using the baseline model parameter values. Since the TSKM model parameters are fitted to match the *in silico* findings of Refoyo et al. [11], both models showed similar concentration profiles and IS clearance values, as shown in Fig. 2A and B, respectively. The clearance was calculated as:

$$\text{Clearance} = \frac{C_{is_d}}{C_{is_b}} \times \frac{V}{AT} \tag{14}$$

where, C_{is_d} was the average of the toxin concentration in the dialysate, C_{is_b} was the toxin concentration at the blood inlet, which was 100 μM, V, the volume of the dialysate, was 0.3 mL, A is the area of the hollow fiber compartment, which was 0.13 cm^2, and T is the time at which the clearance was calculated. Note that C_{is_d} was the average of the concentration albumin-bound and albumin-free IS over the entire dialysate domain and not just at the outlet. Supporting Fig. 4 presents the clearance values of only albumin-bound IS of Jansen et al., compared with the Lumped Model and TSKM. The clearances were calculated by Equation (14) and concentration profiles are slightly lower for TSKM than that observed for the Refoyo kinetics but overall these results indicated that similar clearances can be achieved via multiple types of kinetics models. We focus here on the first 10 min, comparable to Refoyo et al. (Fig. 2A and B).

3.2. Uptake rate, dissociation rate and transporter density have an important influence on the IS clearance

After corroborating the TSKM with the experimental data reported in Refoyo et al. [11], the influence of the uptake rate, dissociation rate and initial transporter density on the IS clearance was explored. Since transporters can be differentially expressed depending on the conditions under which the cell layer was cultured [14,15], it was interesting to explicitly study the influence of the transporter activity and density on the overall toxin clearance (Table 4). Importantly, to the best of the authors' knowledge, this was the first time that the transporter density was modeled explicitly and that the influence thereof on toxin clearance.

Fig. 3Ashowed that the toxin concentration in the dialysate increased with an increase in transporter density. Similar to the other two parameters, the toxin concentration saturated once the number of transporters in the cell monolayer exceeded a particular threshold. The simulation results indicated that an OAT1 density greater than 7e-5 mol m^{-2} would result in a system that has excess transporters and in which, consequently, the IS clearance will not be limited by the OAT1 availability. Interestingly, by decreasing the OAT1 density, we can virtually investigate scenarios where the cells do not express sufficient OAT1, for example, due to dedifferentiation or internalization of OAT1 when the proximal tubule cells are cultured in suboptimal conditions.

Similarly, Fig. 3B showed that the dialysate toxin concentration increased with an increase in the dissociation rate, $k_{f_{unbind}}$. As more toxins

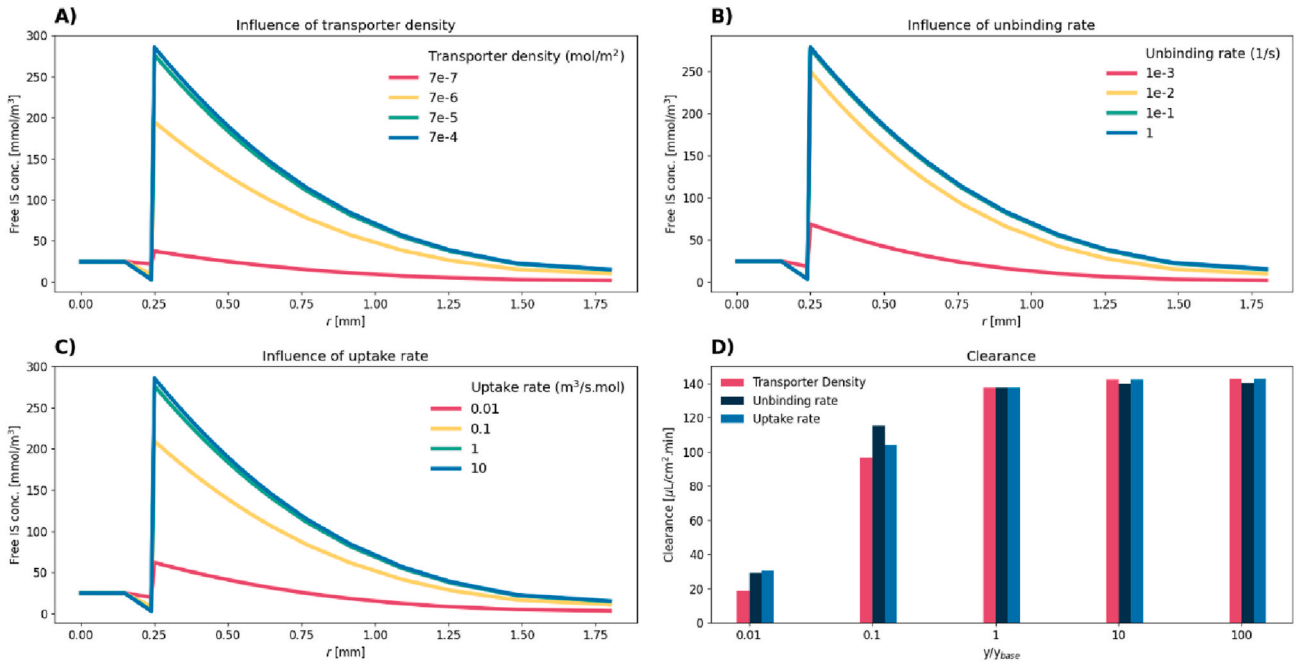

Fig. 3. Panel view comparing the baseline models cross-section at $z = 10$ mm. The y-axis units were converted to mmol m^{-3} to better present the data in graphical format. (A) Effect of varying the initial OAT1 density on the transport of IS from the blood compartment to the dialysis compartment in the presence of albumin at time $t = 10$ min. The initial unbound OAT1 density was varied 7e-4, 7e-5, 7e-6, 7e-7 mol m^{-2} while all the other parameters were kept constant. (B) Effect of varying OAT1 toxin unbind rate on the transport of IS from the blood compartment to the dialysis compartment in the presence of albumin at time $t = 10$ min. The dissociation rate of the toxin from the OAT1 was varied 0.001, 0.01, 0.1, 1 s^{-1}, while all the other parameters were kept constant. (C) Effect of varying OAT1 uptake rate on the transport of IS from the blood compartment to the dialysis compartment in the presence of albumin at time $t = 10$ min. The uptake binding rate of the toxin-albumin complex with the OAT1 was varied 0.01, 0.1, 1 and 10 m^3 s^{-1} mol^{-1} while all the other parameters were kept constant. (D) Clearance rates (µL cm^{-2} min^{-1}) were calculated for all cases defined. y refers to the parameter value, y_{base} is the original parameter value if the TSKM, with $y/y_{base} = 1$ is the original parameter setting for the TSKM. The sensitivity analysis for the parameter changes performed in Fig. 3 can be found in the supporting Fig. 3.

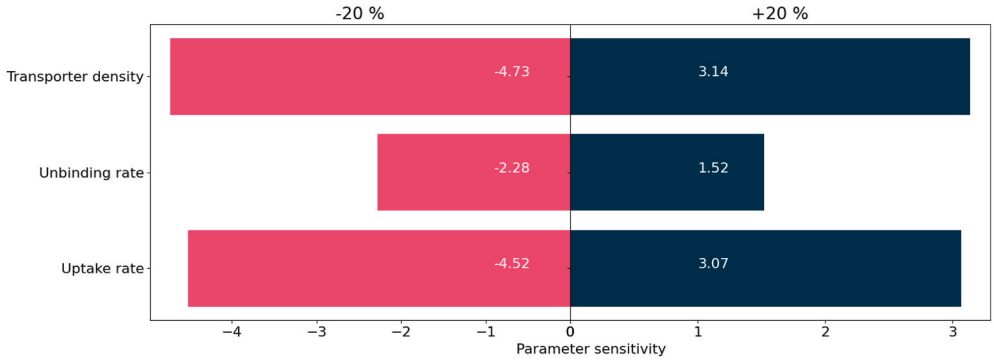

Fig. 4. Sensitivity analysis was performed on the varied parameters with ± 20% changes to the original parameter values stated in Table 1 in the TSKM by comparing the model clearance values at 10 min.

dissociated from the toxin-albumin-OAT complex, there was a higher influx into the dialysate. It was shown that above 0.1 s^{-1}, the OAT1 was saturated and a further increase in the dissociation rate did not affect the final transport. Note that there was a large discrepancy between the lower values of 0.001 and 0.01 s^{-1}, pointing towards non-linear mass transport effects.

Fig. 3C showed that as the uptake rate increased, transport of toxins into the dialysate was increased. This can be explained by the fact that as more toxins were able to bind to the transporters due to the higher uptake rate, the toxin in the dialysate will ultimately be increased. Interestingly, the toxin concentration profile saturated at $k_{f_{uptake}} = 1$ m^3 s^{-1} mol^{-1}, which was the base value. It was assumed here that the free and bound toxins are binding to the transporter at the same rates. There was a large discrepancy between the lower values of 0.01 (red) and 0.1 (yellow) m^3 s^{-1} mol^{-1}. For an uptake rate 0.01 m^3 s^{-1} mol^{-1}, the peak value of the transported IS in the dialysis compartment is 25% of the base model's peak value.

Fig. 3D displayed the calculated clearance for each step change in the TSKM. The clearance increased with an increase in parameter value but saturated finally at 142 µL cm^{-2} min^{-1}. With the parameter values $y = y_{base}$ according to the standard model (OAT_{free} = 7e-5 mol m^{-2}; $k_{f_{uptake}} = 1$ m^3 s^{-1} mol^{-1}; $k_{f_{unbind}} = 0.1$ s^{-1}), the clearance did not improve much upon increasing any of the parameters since the clearance was almost saturated for the standard model settings (OAT_{free} = 7e-5 mol m^{-2}; $k_{f_{uptake}} = 1$ m^3 s^{-1} mol^{-1}; $k_{f_{unbind}} = 0.1$ s^{-1}). This further emphasizes that the kinetics of the toxin transport reaction are at their highest possible rate. To confirm this, the Thiele modulus was calculated, which compared the effect of diffusion with the effect of reaction on the overall toxin clearance. The Thiele modulus for both steps of the TSKM was

calculated as 2.67, indicating that the toxin diffusion was indeed the rate-limiting step (see supplementary material for calculation). If the Thiele modulus was used to back-calculate the transporter density implicitly assumed in the Lumped Model kinetics, we arrive at a transporter density of 0.16 mol m^{-2} (see supplementary material), which was much higher than the base value of the TSKM and points again towards high reaction kinetics and a diffusion-limited system.

The sensitivity analysis results (equation (13)) showed that the most influential parameters on the clearance of IS were the transporter density and the OAT1 uptake rate (Fig. 4). Notably, the TSKM was less sensitive to increasing the parameter values than decreasing them.

3.3. A more uniform distribution of toxin transporters results in a higher clearance

As a next step, we explored whether the transporter distribution influences the clearance in the cell monolayer. Molecular transporter engineering was an often ventured tool to improve metabolism in cells [16,17]. Since we were able to quantify transporter density in the TSKM accurately, the transporter density *in silico* was varied and its influence on toxin transport was studied.

In this section, the multiple variations of the transporter distribution was tested while keeping the total number of transporters constant. 11 specific patterns were simulated as shown in Fig. 5. More specifically, we simulated a uniform monolayer (P1), structures with gaps and a uniform distribution on the remaining patches (P2, P3, P4, P5, P6, P7, P10) and structures with gaps and a non-uniform distribution on the remaining patches (P8, P9, P11). Importantly, we redefined the transporter density distribution such that a constant (total) transporter number was ensured.

As can be seen in Fig. 5, the monolayer (P1) resulted in the maximum clearance. Further, the results indicated that the cell monolayer with the smallest gap (P2) had the next highest clearance. In contrast, in patterns with large areas without toxin transporters such as P11, even with a transporter density of five times that of the base value, the clearance was the lowest of all patterns. When patterns with the same amount of gap area but a different transporter distribution were compared, such as P7 and P8, the pattern with the most homogeneous distribution showed the highest clearance (clearance P7 > clearance P8). However, the difference in clearance was small, indicating that the amount of gap area was more important than the uniformity of transporter density. Interestingly, a comparison of P5 and P6 (same as P11 and P12) indicated that it does not matter whether the monolayer was present in the center or at the edges of the hollow fiber (for the same amount of monolayer area and the same transporter density). In patterns P5, P6, P7 and P8, with a single or multiple gaps but the same transporter density (TD * 2), it was seen that a more homogeneous distribution with multiple gaps (P7 and P8) has a better clearance than solid blocks just the edges (P5) or at the center (P6).

When patterns with varying amounts of gap area were compared, the simulation results indicated that the clearance was inversely proportional to the gap area in the monolayer. These findings reaffirmed that a uniform monolayer culture will provide the highest clearance and underline the importance thereof.

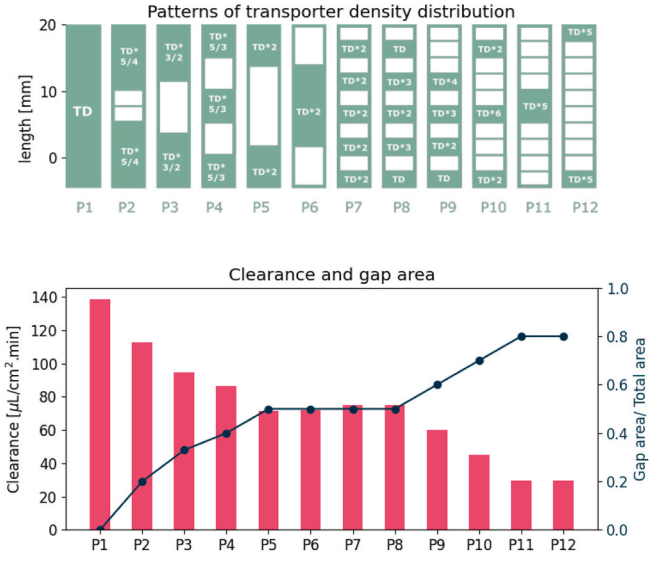

Fig. 5. (Top) Various toxin transporter distribution patterns tested out in the model. TD = the baseline transporter density, 7e-5 mol m^{-2} (Bottom) Clearance of IS at $t = 10$ min for different distributions of transporter density. The blue line plots the gap area (no cells) over the total area.

4. Discussion

In this study, a comparison was made between a two-step binding kinetics model (TSKM) and a lumped parameter model (Lumped Model) to compute IS clearance in a cellularized hollow fiber membrane, as functional unit of a bioartificial kidney. In these *in silico* representations, the toxin IS was assumed to be transported from the blood compartment across the cell membrane by OAT1. The toxin bound to albumin at one site only for which a constant binding rate was assumed. The dissociation from albumin was assumed to be spontaneous at the basolateral side of the membrane. The main difference between the Lumped Model and the TSKM presented in this study lies in how the activity of the transporters was modeled. More specifically, in the TSKM, the transport was broken down into a two-step process in which the albumin-toxin binds to an OAT1, and then the complex dissociated at the basolateral side to release the free toxin into the dialysate.

The two types of kinetics, implemented in COMSOL Multiphysics 5.4, resulted in IS concentration curves that matched with very little deviance in peak values (~17 mol m^{-3}). Furthermore, the clearance values of the two types of models differed only by 8 μL cm^{-2} min^{-1}, and as such, also matched with the *in vitro* data of Refoyo et al. [11] Both the concentration profiles and clearance values provided evidence that the TSKM was able to predict comparable results to the MM lumped parameter model.

When the models were compared, the Lumped Model assumed overexpression of OAT1 and saturation of the transporter. This was a reasonable assumption since the ciPTEC-OAT1 cell line was a genetically modified cell line overexpressing OAT1 [14]. Similarly, the MM used in the Lumped Model as the general inward flux assumed transporter saturation since the substrate initial condition (100 μM IS) was greater than 10 times the K_m value (1 μM) [18,19]. Similarly, since the transport parameters used in the surface reactions were fitted to the *in vitro* data of the Lumped Model, the TSKM also functions at saturation level ($k_{f_{uptake}} = 1$ m^3 s^{-1} mol^{-1}; $k_{f_{unbind}} = 0.1$ s^{-1}) and an overexpression of unbound OAT1 (OAT_{free} = 7e-5 mol m^{-2}). The model saturation was apparent in Fig. 3D, where there was insignificant change in the clearance values between the base model ($y/y_{base} = 1$) and 10 times increase in the base model parameter values ($y/y_{base} = 10$). While, if the base model was compared to a reduction by 10 ($y/y_{base} = 0.1$), there was a substantial decrease in clearance with all the parameter values. Interestingly, in unsaturated conditions, the transporter density became the most essential parameter to achieve an optimum clearance of IS, while IS uptake and dissociation rate by the transporter result in similar contributions to IS clearance, as presented in Supporting Fig. 1.

Importantly, the TSKM allowed modeling of the number of transporters and their activity independently. More specifically, by separating the kinetics, it was possible to study the individual effects of the binding and uptake rate and transporter density. Using a sensitivity analysis (Fig. 4), we observed that the most influential parameters were the transporter density and uptake rate of the transporter. This indicated

that the limiting factor at low clearance scenarios was the number of available transporters (transporter density) and their functionality to take up the IS (uptake rate).

As the transporter density was observed to be the most dominant parameter in Fig. 4, the impact of its distribution along the hollow fiber was investigated by considering different layouts for the transporter distribution. Such scenarios may be encountered when the proximal tubule cells are cultured in varied environments leading to sub-optimal expression of OAT1 or areas along the epithelial monolayer with impaired OAT1 function. When a constant transporter number was assumed, the simulation results showed that a uniform monolayer culture provides the optimum result with maximal toxin clearance out of all 11 patterns tested. In addition, a sequence of shorter monolayer patches was more efficient than a long monolayer of the same total length. The above results have important design implications for the hollow fiber membranes as functional units of the BAK. Firstly, longer monolayers are more difficult to culture because of high contractility forces produced by confluent cells resulting in the monolayer detaching form the 3D substrate [20,21]. The results from this study suggest that smaller cell culture units or modules are more functional and robust – a concept, which was fully in line with and supports e.g. the parallelization and multiplexing strategies of miniaturized lab- or organ-on-chip devices [22–25]. Future work should focus on understanding how the kidney epithelium would respond to local damage, e.g. through wound healing processes that restore the monolayer (as suggested by the computational results) or by upregulating the transporter density in the unaffected areas. In addition, *in vitro* wound (scratch) assays could be used to determine the critical size of a local defect in the cell monolayer, which could not be restored and could lead to problems with the clinical safety of the BAK.

As with all models, the results of this study should be interpreted in light of the assumptions and simplifications of both the Lumped Model [11] and the TSKM. Firstly, both models represented the interaction between only one toxin (IS) and one transporter (OAT1), despite there being over 130 characterized uremic toxins and over 400 genetically identified epithelial transporters [8]. Secondly, the models did not account for metabolite and toxin competition for the OAT1. Similarly, the models did not account for the albumin binding kinetics and potential conformational changes occurring in diseased states such as uremic conditions in kidney failure [26]. Both models assumed that the albumin and albumin-bound IS were constantly in equilibrium with $K_{eq} = 377$ mol m^{-3} and that the diffusion coefficient of bound and free IS were the same. This was done to create comparable models between the TSKM and the Lumped Model [11]. Thirdly, the models assumed that the unbound and bound IS had the same binding affinity to OAT1 in order to fairly compare the previously published Lumped Model and the TSKM. The binding affinities are shown to be different [27] and the models should be modified later upon availability of time series experimental data. The models also assumed an overexpression of OAT1, which may be an overestimation as transporter expression was typically reduced in cell cultures. Lastly, the Lumped Model and TSKM were compared with the experimentally measured clearance of albumin-bound IS of Jansen et al. [10] (Supporting Fig. 4). It can be seen that there is a difference in clearance values between the experimental data point and the two computational models. We think the reason for this difference might be an overestimation of the transporter density used for the TSKM (as it was fitted to match the Lumped Model). As such, future work should focus on measuring the transporter density experimentally to further validate the TSKM. We strongly suggest that both the Lumped Model and TSKM should be validated with multiple experimental time points to fully capture the biological complexity of the IS interactions with OAT1. In addition, a global sensitivity analysis, varying multiple varying parameters at the same time, could further improve the understanding of the most influential parameter values and their interactions. The model should be extended to include the radial distribution of transporter to observe the both the lateral and radial effect of transporter distribution along the hollow fiber and around it.

Despite the above mentioned limitations, the Lumped Model and the TSKM can be compared because the models difference lies in the boundary condition definition. The results of this manuscript indicate that both transporter-dependent and –independent flux boundary conditions can help in predicting toxin clearance for bioartificial kidney research. On the one hand, the TSKM model provides the opportunity to investigate the influence of sex differences [28], flow rate [29] or drug concentration [30] on transporter expression and toxin removal function. On the other hand, if these variables do not influence the transporter expression significantly, a lumped model would be an excellent alternative to investigate the overall system kinetics with the advantage of simplicity.

5. Conclusion

In summary, we have developed a model using TSKM to separate, for the first time, the OAT1 functionality from its expression. The model can be used to investigate further different perspectives of toxin transport in a cell-laden hollow-fiber system [10]. More specifically, we have shown that the TSKM was comparable to a lumped parameter model described previously [11]. We were able to modulate the transporter functionality and density independently and modeled their influence on IS clearance without affecting the computational speed. We showed that a monolayer with uniform transporter density maximizes the IS clearance by modifying the transporter density and distribution. As such, the model results highlight the importance of capturing the individual binding kinetics, rather than lumping them together, in order to improve our understanding of toxin transport in bioengineered cell-laden hollow fibers. Moreover, the model results have important design implications for the hollow fiber membranes for the BAK, i.e. shorter, serially connected cell cultures would be more viable, functionally easier to handle *in vitro,* and more robust. This study illustrated that the model can aid in designing promising future renal replacement therapies in conjunction with laboratory experiments.

Declaration of competing interest

The authors declare that they have no known competing financial interests or personal relationships that could have appeared to influence the work reported in this paper.

Acknowledgments

We would like to thank R. Refoyo, E. Skouras and V. Burganos for the help with the model implementation in COMSOL Multiphysics 5.4 and Z. Karagöz for the independent model checking. J. King is responsible for conceptualization, model implementation, results analysis, and manuscript writing. S. Swapnasrita is responsible for the model implementation, results analysis and manuscript writing. A. Carlier, R. Truckenmüller, and S. Giselbrecht are responsible for conceptualization, manuscript revision, and securing funding. R. Masereeuw responsible for conceptualization and manuscript revision.

Appendix A. Supplementary data

Supplementary data to this article can be found online at https://doi.org/10.1016/j.compbiomed.2021.104912.

Funding

This work is supported by the partners of Regenerative Medicine Crossing Borders (RegMed XB), a public-private partnership that uses regenerative medicine strategies to cure common chronic diseases. This collaboration project is financed by the Dutch Ministry of Economic Affairs by means of the PPP allowance made available by the Top Sector

Life Sciences & Health to stimulate public-private partnerships.

References

[1] B. Bikbov, C.A. Purcell, A.S. Levey, M. Smith, A. Abdoli, M. Abebe, O.M. Adebayo, et al., Lancet (2020) 395.
[2] J.S. Berns, Am. J. Kidney Dis. 66 (2015) 547–551.
[3] R. Vanholder, U. Baurmeister, P. Brunet, G. Cohen, G. Glorieux, J. Jankowski, J. Am. Soc. Nephrol. 19 (2008).
[4] R. Masereeuw, H.A.M. Mutsaers, T. Toyohara, T. Abe, S. Jhawar, D.H. Sweet, J. Lowenstein, Semin. Nephrol. 34 (2014).
[5] J. Jansen, J. Jankowski, P.R. Gajjala, J.F.M. Wetzels, R. Masereeuw, Clin. Sci. (2017) 131.
[6] F. Duranton, G. Cohen, R. De Smet, M. Rodriguez, J. Jankowski, R. Vanholder, A. Argiles, J. Am. Soc. Nephrol. 23 (2012).
[7] A. Yavuz, C. Tetta, F.F. Ersoy, V. D'Intini, R. Ratanarat, M. De Cal, M. Bonello, V. Bordoni, G. Salvatori, E. Andrikos, G. Yakupoglu, N.W. Levin, C. Ronco, Semin. Dial. (2005) 18.
[8] K.M. Giacomini, S.M. Huang, D.J. Tweedie, L.Z. Benet, K.L.R. Brouwer, X. Chu, A. Dahlin, R. Evers, V. Fischer, K.M. Hillgren, K.A. Hoffmaster, T. Ishikawa, D. Keppler, R.B. Kim, C.A. Lee, M. Niemi, J.W. Polli, Y. Sugiyama, P.W. Swaan, J. A. Ware, S.H. Wright, S. Wah Yee, M.J. Zamek-Gliszczynski, L. Zhang, Nat. Rev. Drug Discov. 9 (2010).
[9] H. A. M. Mutsaers, L. P. van den Heuvel, L. H. J. Ringens, A. C. A. Dankers, F. G. M. Russel, J. F. M. Wetzels, J. G. Hoenderop and R. Masereeuw, PLoS One, , DOI: 10.1371/journal.pone.0018438.
[10] J. Jansen, M. Fedecostante, M.J. Wilmer, J.G. Peters, U.M. Kreuser, P.H. Van Den Broek, R.A. Mensink, T.J. Boltje, D. Stamatialis, J.F. Wetzels, L.P. Van Den Heuvel, J.G. Hoenderop, R. Masereeuw, Sci. Rep. 6 (2016).
[11] R. Refoyo, E.D. Skouras, N.V. Chevtchik, D. Stamatialis, V.N. Burganos, J. Membr. Sci. (2018) 565.
[12] K.P. Lehre, N.C. Danbolt, J. Neurosci. 18 (1998).
[13] C. Cruickhank Miller, Proc. Roy. Soc. Lond. A 17 (1924).
[14] M.J. Wilmer, M.A. Saleem, R. Masereeuw, L. Ni, T.J. Van Der Velden, F.G. Russel, P.W. Mathieson, L.A. Monnens, L.P. Van Den Heuvel, E.N. Levtchenko, Cell Tissue Res. 339 (2009).
[15] M. Bens and A. Vandewalle, Eur. J. Physiol., , DOI:10.1007/s00424-008-0507-4.
[16] E.M. Young, A.D. Comer, H. Huang, H.S. Alper, Metab. Eng. (2012) 14.
[17] C. Zhang, X. Chen, G. Stephanopoulos, H.P. Too, Biotechnol. Bioeng. (2016) 113.
[18] J.K. Kim, J.J. Tyson, PLoS Comput. Biol. (2020) 16.
[19] B. Choi, G.A. Rempala, J.K. Kim, Sci. Rep. 7 (2017).
[20] T. Yamashita, P. Kollmannsberger, K. Mawatari, T. Kitamori, V. Vogel, Acta Biomater. 45 (2016).
[21] F. Hulshof, C. Schophuizen, M. Mihajlovic, C. van Blitterswijk, R. Masereeuw, J. de Boer, D. Stamatialis, J. Tissue Eng. Regen. Med. 12 (2018).
[22] J. Rogal, C. Probst and P. Loskill, 2017, 3.
[23] R. Paoli and J. Samitier, Micromachines, , DOI:10.3390/mi7070126.
[24] L. A. Low, C. Mummery, B. R. Berridge, C. P. Austin and D. A. Tagle, Nat. Rev. Drug Discov., , DOI:10.1038/s41573-020-0079-3.
[25] P. Neužil, S. Giselbrecht, T.J. Huang, M.S. Complex, Nat. Rev. Drug Discov. (2012) 11.
[26] W.R. Clark, N.L. Dehghani, V. Narsimhan, C. Ronco, Blood Purif. 48 (2019).
[27] T.K. Van Der Made, M. Fedecostante, D. Scotcher, A. Rostami-Hodjegan, J. Sastre Toranō, I. Middel, A.S. Koster, K.G. Gerritsen, V. Jankowski, J. Jankowski, J.G. J. Hoenderop, R. Masereeuw, A. Galetin, Mol. Pharm. 16 (2019).
[28] R. Hu, A.A. McDonough, A.T. Layton, Am. J. Physiol. Ren. Physiol. (2020) 319.
[29] A.T. Layton, H.E. Layton, PLoS Comput. Biol. 15 (2019).
[30] A. M. Weinstein, Am. J. Physiol. Ren. Physiol., , DOI:10.1152/ajprenal.00043.2005.